Supplementary Material for Surface Networks

Ilya Kostrikov, Zhongshi Jiang, Daniele Panozzo, Denis Zorin, Joan Bruna
New York University

March 29, 2018

Abstract

This note contains the appendices of the paper Surface Networks.

A The Dirac Operator

The quaternions $\mathbb{H}$ is an extension of complex numbers. A quaternion $q \in \mathbb{H}$ can be represented in a form $q = a + bi + cj + dk$ where a, b, c, d are real numbers and i, j, k are quaternion units that satisfy the relationship $i^2 = j^2 = k^2 = ijk = -1$.

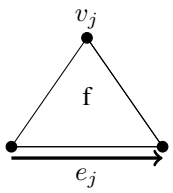

As mentioned in Section 3.1, the Dirac operator used in the model can be conveniently represented as a quaternion matrix:

$$D_{f,j} = \frac{-1}{2|\mathcal{A}_f|} e_j \ , \ f \in F, j \in V \ ,$$

where e_j is the opposing edge vector of node j in the face f, and $\mathcal{A}_f$ is the area, as illustrated in Fig. A, using counter-clockwise orientations on all faces.

The Deep Learning library PyTorch that we used to implement the models does not support quaternions. Nevertheless, quaternion-valued matrix multiplication can be replaced with real-valued matrix multiplication where each entry $q = a + bi + cj + dk$ is represented as a 4×4 block

$$\begin{bmatrix} a & -b & -c & -d \\ b & a & -d & c \\ c & d & a & -b \\ d & -c & b & a \end{bmatrix}$$

and the conjugate $q^* = a - bi - cj - dk$ is a transpose of this real-valued matrix:

$$\begin{bmatrix} a & b & c & d \\ -b & a & d & -c \\ -c & -d & a & b \\ -d & c & -b & a \end{bmatrix} .$$

B Theorem 4.1

B.1 Proof of (a)

We first show the result for the mapping $x \mapsto \rho\,(Ax + B\Delta x)$, corresponding to one layer of Φ_Δ. By definition, the Laplacian Δ of $\mathcal{M}$ is

$$\Delta = \text{diag}(\bar{\mathcal{A}})^{-1}(U - W)\;,$$

where $\bar{\mathcal{A}}_j$ is one third of the total area of triangles incident to node j, and $W = (w_{i,j})$ contains the cotangent weights [9], and $U = \text{diag}(W\mathbf{1})$ contains the node aggregated weights in its diagonal.

From [4] we verify that

$$\begin{aligned} \|U - W\| &\leq \sqrt{2}\max_i \left\{ \sqrt{U_i^2 + U_i \sum_{i\sim j} U_j w_{i,j}} \right\} \\ &\leq 2\sqrt{2}\sup_{i,j} w_{i,j} \sup_j d_j \\ &\leq 2\sqrt{2}\cot(\alpha_{\min}) d_{\max}\;, \end{aligned} \tag{1}$$

where d_j denotes the degree (number of neighbors) of node j, $\alpha_{\min}$ is the smallest angle in the triangulation of $\mathcal{M}$ and $S_{\max}$ the largest number of incident triangles. It results that

$$\|\Delta\| \leq C\frac{\cot(\alpha_{\min}) S_{\max}}{\inf_j \bar{\mathcal{A}}_j} := L_{\mathcal{M}}\;,$$

which depends uniquely on the mesh $\mathcal{M}$ and is finite for non-degenerate meshes. Moreover, since $\rho(\,\cdot\,)$ is non-expansive, we have

$$\begin{aligned} \|\rho\,(Ax + B\Delta x) - \rho\,(Ax' + B\Delta x')\| &\leq \|A(x - x') + B\Delta(x - x')\| \\ &\leq (\|A\| + \|B\|L_{\mathcal{M}})\|x - x'\|\;. \end{aligned} \tag{2}$$

By cascading (2) across the K layers of the network, we obtain

$$\|\Phi(\mathcal{M}; x) - \Phi(\mathcal{M}; x')\| \leq \left(\prod_{k\leq K} (\|A_k\| + \|B_k\|L_{\mathcal{M}}) \right) \|x - x'\|\;,$$

which proves (a). □

B.2 Proof of (b)

The proof is analogous, by observing that $\|D\| = \sqrt{\|\Delta\|}$ and therefore

$$\|D\| \leq \sqrt{L_{\mathcal{M}}}\;.\quad \square$$

B.3 Proof of (c)

To establish (c) we first observe that given three points $p, q, r \in \mathbb{R}^3$ forming any of the triangles of $\mathcal{M}$,

$$\|p - q\|^2(1 - |\nabla\tau|_\infty)^2 \leq \|\tau(p) - \tau(q)\|^2 \leq \|p - q\|^2(1 + |\nabla\tau|_\infty)^2 \tag{3}$$

$$\mathcal{A}(p,q,r)^2(1 - |\nabla\tau|_\infty C\alpha_{\min}^{-2} - o(|\nabla\tau|_\infty{}^2)) \leq \mathcal{A}(\tau(p),\tau(q),\tau(r))^2 \leq \mathcal{A}(p,q,r)^2(1 + |\nabla\tau|_\infty C\alpha_{\min}^{-2} + o(|\nabla\tau|_\infty{}^2)) \tag{4}$$

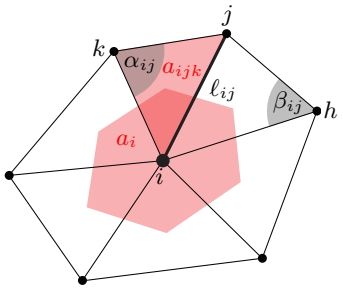

Figure 1: Triangular mesh and Cotangent Laplacian (figure reproduced from [2])

Indeed, (3) is a direct consequence of the lower and upper Lipschitz constants of $\tau(u)$, which are bounded respectively by $1-|\nabla\tau|_\infty$ and $1+|\nabla\tau|_\infty$. As for (4), we use the Heron formula

$$\mathcal{A}(p,q,r)^2 = s(s-\|p-q\|)(s-\|p-r\|)(s-\|r-q\|)\ ,$$

with $s=\frac{1}{2}(\|p-q\|+\|p-r\|+\|r-q\|)$ being the half-perimeter. By denoting s_τ the corresponding half-perimeter determined by the deformed points $\tau(p),\tau(q),\tau(r)$, we have that

$$s_\tau - \|\tau(p)-\tau(q)\| \leq s(1+|\nabla\tau|_\infty) - \|p-q\|(1-|\nabla\tau|_\infty) = s-\|p-q\|+|\nabla\tau|_\infty(s+\|p-q\|) \text{ and}$$

$$s_\tau - \|\tau(p)-\tau(q)\| \geq s(1-|\nabla\tau|_\infty) - \|p-q\|(1+|\nabla\tau|_\infty) = s-\|p-q\|-|\nabla\tau|_\infty(s+\|p-q\|)\ ,$$

and similarly for the $\|r-q\|$ and $\|r-p\|$ terms. It results in

$$\begin{aligned}\mathcal{A}(\tau(p),\tau(q),\tau(r))^2 &\geq \mathcal{A}(p,q,r)^2\left[1-|\nabla\tau|_\infty\left(1+\frac{s+\|p-q\|}{s-\|p-q\|}+\frac{s+\|p-r\|}{s-\|p-r\|}+\frac{s+\|r-q\|}{s-\|r-q\|}\right)-o(|\nabla\tau|_\infty{}^2)\right]\\ &\geq \mathcal{A}(p,q,r)^2\left[1-C|\nabla\tau|_\infty\alpha_{\min}^{-2}-o(|\nabla\tau|_\infty{}^2)\right]\ ,\end{aligned}$$

and similarly

$$\mathcal{A}(\tau(p),\tau(q),\tau(r))^2 \leq \mathcal{A}(p,q,r)^2\left[1+C|\nabla\tau|_\infty\alpha_{\min}^{-2}-o(|\nabla\tau|_\infty{}^2)\right]\ .$$

By noting that the cotangent Laplacian weights can be written (see Fig. 1) as

$$w_{i,j} = \frac{-\ell_{ij}^2+\ell_{jk}^2+\ell_{ik}^2}{\mathcal{A}(i,j,k)} + \frac{-\ell_{ij}^2+\ell_{jh}^2+\ell_{ih}^2}{\mathcal{A}(i,j,h)}\ ,$$

we have from the previous Bilipschitz bounds that

$$\tau(w_{i,j}) \leq w_{i,j}\left[1-C|\nabla\tau|_\infty\alpha_{\min}^{-2}\right]^{-1} + 2|\nabla\tau|_\infty\left[1-C|\nabla\tau|_\infty\alpha_{\min}^{-2}\right]^{-1}\left(\frac{\ell_{ij}^2+\ell_{jk}^2+\ell_{ik}^2}{\mathcal{A}(i,j,k)}+\frac{\ell_{ij}^2+\ell_{jh}^2+\ell_{ih}^2}{\mathcal{A}(i,j,h)}\right)\ ,$$

$$\tau(w_{i,j}) \geq w_{i,j}\left[1+C|\nabla\tau|_\infty\alpha_{\min}^{-2}\right]^{-1} - 2|\nabla\tau|_\infty\left[1+C|\nabla\tau|_\infty\alpha_{\min}^{-2}\right]^{-1}\left(\frac{\ell_{ij}^2+\ell_{jk}^2+\ell_{ik}^2}{\mathcal{A}(i,j,k)}+\frac{\ell_{ij}^2+\ell_{jh}^2+\ell_{ih}^2}{\mathcal{A}(i,j,h)}\right)\ ,$$

which proves that, up to second order terms, the cotangent weights are Lipschitz continuous to deformations.

Finally, since the mesh Laplacian operator is constructed as $\mathrm{diag}(\bar{\mathcal{A}})^{-1}(U-W)$, with $\bar{\mathcal{A}}_{i,i} = \frac{1}{3}\sum_{j,k;(i,j,k)\in F}\mathcal{A}(i,j,k)$, and $U = \mathrm{diag}(W\mathbf{1})$, let us show how to bound $\|\Delta - \tau(\Delta)\|$ from

$$\bar{\mathcal{A}}_{i,i}(1-\alpha_{\mathcal{M}}|\nabla\tau|_\infty - o(|\nabla\tau|_\infty{}^2)) \leq \tau(\bar{\mathcal{A}}_{i,i}) \leq \bar{\mathcal{A}}_{i,i}(1+\alpha_{\mathcal{M}}|\nabla\tau|_\infty + o(|\nabla\tau|_\infty{}^2)) \quad (5)$$

and

$$w_{i,j}(1-\beta_{\mathcal{M}}|\nabla\tau|_\infty - o(|\nabla\tau|_\infty{}^2)) \leq \tau(w_{i,j}) \leq w_{i,j}(1+\beta_{\mathcal{M}}|\nabla\tau|_\infty + o(|\nabla\tau|_\infty{}^2)) \,. \quad (6)$$

Using the fact that $\bar{\mathcal{A}}$, $\tau(\bar{\mathcal{A}})$ are diagonal, and using the spectral bound for $k\times m$ sparse matrices from [3], Lemma 5.12,

$$\|Y\|^2 \leq \max_i \sum_{j;\, Y_{i,j}\neq 0} |Y_{i,j}| \left(\sum_{r=1}^{l} |Y_{r,j}|\right) \,,$$

the bounds (5) and (6) yield respectively

$$\begin{aligned} \tau(\bar{\mathcal{A}}) &= \bar{\mathcal{A}}(\mathbf{1}+\epsilon_\tau) \,, \text{ with } \|\epsilon_\tau\| = o(|\nabla\tau|_\infty) \,, \text{and} \\ \tau(U-W) &= U - W + \eta_\tau \,, \text{ with } \|\eta_\tau\| = o(|\nabla\tau|_\infty) \,. \end{aligned}$$

It results that, up to second order terms,

$$\begin{aligned} \|\Delta - \tau(\Delta)\| &= \left\|\tau(\bar{\mathcal{A}})^{-1}(\tau(U)-\tau(W)) - \bar{\mathcal{A}}^{-1}(U-W)\right\| \\ &= \left\|\left(\bar{\mathcal{A}}[\mathbf{1}+\epsilon_\tau]\right)^{-1}[U-W+\eta_\tau] - \bar{\mathcal{A}}^{-1}(U-W)\right\| \\ &= \left\|\left(\mathbf{1}-\epsilon_\tau + o(|\nabla\tau|_\infty{}^2)\right)\bar{\mathcal{A}}^{-1}(U-W+\eta_\tau) - \bar{\mathcal{A}}^{-1}(U-W)\right\| \\ &= \left\|\epsilon_\tau\Delta + \bar{\mathcal{A}}^{-1}\eta_\tau\right\| + o(|\nabla\tau|_\infty{}^2) \\ &= o(|\tau|_\infty) \,, \end{aligned}$$

which shows that the Laplacian is stable to deformations in operator norm. Finally, by denoting $\tilde{x}_\tau$ a layer of the deformed Laplacian network

$$\tilde{x}_\tau = \rho(Ax + B\tau(\Delta)x) \,,$$

it follows that

$$\begin{aligned} \|\tilde{x} - \tilde{x}_\tau\| &\leq \|B(\Delta - \tau(\Delta)x\| & (7) \\ &\leq C\|B\||\nabla\tau|_\infty\|x\| \,. & (8) \end{aligned}$$

Also,

$$\begin{aligned} \|\tilde{x} - \tilde{y}_\tau\| &\leq \|A(x-y) + B(\Delta x - \tau(\Delta)y)\| \\ &\leq (\|A\| + \|B\|\|\Delta\|)\|x-y\| + \|\Delta - \tau(\Delta)\|\|x\| \\ &\leq \underbrace{(\|A\| + \|B\|\|\Delta\|)}_{\delta_1}\|x-y\| + \underbrace{C|\nabla\tau|_\infty}_{\delta_2}\|x\| \,, & (9) \end{aligned}$$

and therefore, by plugging (9) with $y = \tilde{x}_\tau$, K layers of the Laplacian network satisfy

$$\begin{aligned} \|\Phi(x;\Delta) - \Phi(x;\tau(\Delta)\| &\leq \left(\prod_{j\leq K-1}\delta_1(j)\right)\|\tilde{x}-\tilde{x}_\tau\| + \left(\sum_{j<K-1}\prod_{j'\leq j}\delta_1(j')\delta_2(j)\right)|\nabla\tau|_\infty\|x\| \\ &\leq \left[C\left(\prod_{j\leq K-1}\delta_1(j)\right)\|B\| + \left(\sum_{j<K-1}\prod_{j'\leq j}\delta_1(j')\delta_2(j)\right)\right]|\nabla\tau|_\infty\|x\| \,. \quad \square \,. \end{aligned}$$

B.4 Proof of (d)

The proof is also analogous to the proof of (c), with the difference that now the Dirac operator is no longer invariant to orthogonal transformations, only to translations. Given two points p, q, we verify that

$$\|p - q - \tau(p) - \tau(q)\| \leq \widetilde{|\tau|}_\infty \|p - q\| \,,$$

which, following the previous argument, leads to

$$\|D - \tau(D)\| = o(\widetilde{|\tau|}_\infty) \,. \tag{10}$$

C Theorem 4.2

C.1 Proof of part (a)

The proof is based on the following lemma:

Lemma C.1 *Let $x_N, y_N \in \mathcal{H}(\mathcal{M}_N)$ such that $\forall\, N$, $\|x_N\|_{\mathcal{H}} \leq c, \|y_N\|_{\mathcal{H}} \leq c$. Let $\hat{x_N} = \mathcal{E}_N(x_N)$, where $\mathcal{E}_N$ is the eigendecomposition of the Laplacian operator Δ_N on $\mathcal{M}_N$, , with associated eigenvalues $\lambda_1 \ldots \lambda_N$ in increasing order. Let $\gamma > 0$ and β be defined as in (**??**) for x_N and y_N. If $\beta > 1$ and $\|x_N - y_N\| \leq \epsilon$ for all N,*

$$\|\Delta_N(x_N - y_N)\|^2 \leq C\epsilon^{2 - \frac{1}{\beta - 1/2}} \,, \tag{11}$$

where C is a constant independent of ϵ and N.

One layer of the network will transform the difference $x_1 - x_2$ into $\rho(Ax_1 + B\Delta x_1) - \rho(Ax_2 + B\Delta x_2)$. We verify that

$$\|\rho(Ax_1 + B\Delta x_1) - \rho(Ax_2 + B\Delta x_2)\| \leq \|A\|\|x_1 - x_2\| + \|B\|\|\Delta(x_1 - x_2)\| \,.$$

We now apply Lemma C.1 to obtain

$$\begin{aligned}
\|\rho(Ax_1 + B\Delta x_1) - \rho(Ax_2 + B\Delta x_2)\| &\leq \|A\|\|x_1 - x_2\| + C\|B\|\|x_1 - x_2\|^{\frac{\beta-1}{\beta-1/2}} \\
&\leq \|x_1 - x_2\|^{\frac{\beta-1}{\beta-1/2}} \left(\|A\|\|x_1 - x_2\|^{(2\beta-1)^{-1}} + C\|B\| \right) \\
&\leq C(\|A\| + \|B\|)\|x_1 - x_2\|^{\frac{\beta-1}{\beta-1/2}} \,,
\end{aligned}$$

where we redefine C to account for the fact that $\|x_1 - x_2\|^{(2\beta-1)^{-1}}$ is bounded. We have just showed that

$$\|x_1^{(r+1)} - x_2^{(r+1)}\| \leq f_r \|x_1^{(r)} - x_2^{(r)}\|^{g_r} \tag{12}$$

with $f_r = C(\|A_r\| + \|B_r\|)$ and $g_r = \frac{\beta_r - 1}{\beta_r - 1/2}$. By cascading (12) for each of the R layers we thus obtain

$$\|\Phi_\Delta(x_1) - \Phi_\Delta(x_2)\| \leq \left[\prod_{r=1}^{R} f_r^{\prod_{r'>r} g_{r'}} \right] \|x_1 - x_2\|^{\prod_{r=1}^{R} g_r} \,, \tag{13}$$

which proves (**??**) $\square$.

Proof of (11): Let $\{e_1, \dots, e_N\}$ be the eigendecomposition of Δ_N. For simplicity, we drop the subindex N in the signals from now on. Let $\hat{x}(k) = \langle x, e_k \rangle$ and $\tilde{x}(k) = \lambda_k \hat{x}(k)$; and analogously for y. From the Parseval identity we have that $\|x\|^2 = \|\hat{x}\|^2$. We express $\|\Delta(x-y)\|$ as

$$\|\Delta(x-y)\|^2 = \sum_{k \leq N} \lambda_k^2 (\hat{x}(k) - \hat{y}(k))^2 \,. \tag{14}$$

The basic principle of the proof is to cut the spectral sum (14) in two parts, chosen to exploit the decay of $\tilde{x}(k)$. Let

$$F(x)(k) = \frac{\sum_{k' \geq k} \tilde{x}(k)^2}{\|x\|_{\mathcal{H}}^2} = \frac{\sum_{k' \geq k} \tilde{x}(k)^2}{\sum_{k'} \tilde{x}(k)^2} = \frac{\sum_{k' \geq k} \lambda_k^2 \hat{x}(k)^2}{\sum_{k'} \lambda_k^2 \hat{x}(k)^2} \leq 1 \,,$$

and analogously for y. For any cutoff $k_* \leq N$ we have

$$\begin{aligned} \|\Delta(x-y)\|^2 &= \sum_{k \leq k_*} \lambda_k^2 (\hat{x}(k) - \hat{y}(k))^2 + \sum_{k > k_*} \lambda_k^2 (\hat{x}(k) - \hat{y}(k))^2 \\ &\leq \lambda_{k_*}^2 \epsilon^2 + 2(F(x)(k_*)\|x\|_{\mathcal{H}}^2 + F(y)(k_*)\|y\|_{\mathcal{H}}^2) \\ &\leq \lambda_{k_*}^2 \epsilon^2 + 2F(k_*)(\|x\|_{\mathcal{H}}^2 + \|y\|_{\mathcal{H}}^2) \\ &\leq \lambda_{k_*}^2 \epsilon^2 + 4F(k_*)D^2 \,, \end{aligned} \tag{15}$$

where we denote for simplicity $F(k_*) = \max(F(x)(k_*),\ F(y)(k_*))$. By assumption, we have $\lambda_k^2 \lesssim k^{2\gamma}$ and

$$F(k) \lesssim \sum_{k' \geq k} k^{2(\gamma-\beta)} \simeq k^{1+2(\gamma-\beta)} \,.$$

By denoting $\tilde{\beta} = \beta - \gamma - 1/2$, it follows that

$$\|\Delta(x-y)\|^2 \lesssim \epsilon^2 k_*^{2\gamma} + 4D^2 k_*^{-2\tilde{\beta}} \tag{16}$$

Optimizing for k_* yields

$$\epsilon^2 2\gamma k^{2\gamma-1} - 2\tilde{\beta} 4D^2 k^{-2\tilde{\beta}-1} = 0, \text{ thus}$$

$$k_* = \left\lceil \frac{4\beta D^2}{\gamma \epsilon^2} \right\rceil^{\frac{1}{2\gamma+2\tilde{\beta}}} \,. \tag{17}$$

By plugging (17) back into (16) and dropping all constants independent of N and ϵ, this leads to

$$\|\Delta(x-y)\|^2 \lesssim \epsilon^{2-\frac{1}{\gamma+\tilde{\beta}}} = \epsilon^{2-\frac{1}{\beta-1/2}} \,,$$

which proves part (a) $\square$.

C.2 Proof of part (b)

We will use the following lemma:

Lemma C.2 *Let $\mathcal{M} = (V, E, F)$ is a non-degenerate mesh, and define*

$$\eta_1(\mathcal{M}) = \sup_{(i,j) \in E} \frac{\bar{\mathcal{A}}_i}{\bar{\mathcal{A}}_j} \,,\ \eta_2(\mathcal{M}) = \sup_{(i,j,k) \in F} \frac{\ell_{ij}^2 + \ell_{jk}^2 + \ell_{ik}^2}{\mathcal{A}(i,j,k)} \,,\ \eta_3(\mathcal{M}) = \alpha_{min} \,. \tag{18}$$

Then, given a smooth deformation τ and x defined in $\mathcal{M}$, we have

$$\|(\Delta - \tau(\Delta))x\| \leq C|\nabla\tau|_\infty \|\Delta x\| \,, \tag{19}$$

where C depends only upon η_1, η_2 and η_3.

In that case, we need to control the difference $\rho(Ax + B\Delta x) - \rho(Ax + B\tau(\Delta)x)$. We verify that

$$\|\rho(Ax + B\Delta x) - \rho(Ax + B\tau(\Delta)x)\| \leq \|B\|\|(\Delta - \tau(\Delta))x\| \,.$$

By Lemma C.2 it follows that $\|(\Delta - \tau(\Delta))x\| \leq C|\nabla\tau|_\infty\|\Delta x\|$ and therefore, by denoting $x_1^{(1)} = \rho(Ax + B\Delta x)$ and $x_2^{(1)} = \rho(Ax + B\tau(\Delta)x)$, we have

$$\|x_1^{(1)} - x_2^{(1)}\| \leq C|\nabla\tau|_\infty\|\Delta x\| = C|\nabla\tau|_\infty\|x\|_{\mathcal{H}} \,. \tag{20}$$

By applying again Lemma C.1, we also have that

$$\begin{aligned}
\|\Delta x_1^{(1)} - \tau(\Delta)x_2^{(1)}\| &= \|\Delta x_1^{(1)} - (\Delta + \tau(\Delta) - \Delta)x_2^{(1)}\| \\
&= \|\Delta(x_1^{(1)} - x_2^{(1)}) + (\tau(\Delta) - \Delta)x_2^{(1)}\| \\
&\leq C\|x_1^{(1)} - x_2^{(1)}\|^{\frac{\beta_1 - 1}{\beta_1 - 1/2}} + |\nabla\tau|_\infty\|x_2^{(1)}\|_{\mathcal{H}} \\
&\lesssim C|\nabla\tau|_\infty{}^{\frac{\beta_1 - 1}{\beta_1 - 1/2}} \,,
\end{aligned}$$

which, by combining it with (20) and repeating through the R layers yields

$$\|\Phi_\Delta(x, \mathcal{M}) - \Phi_\Delta(x, \tau(\mathcal{M})\| \leq C|\nabla\tau|_\infty{}^{\prod_{r=1}^R \frac{\beta_r - 1}{\beta_r - 1/2}} \,, \tag{21}$$

which concludes the proof □.

Proof of (19): The proof follows closely the proof of Theorem **??**, part (c). From (5) and (6) we have that

$$\begin{aligned}
\tau(\bar{\mathcal{A}}) &= \bar{\mathcal{A}}(\mathbf{I} + G_\tau) \,, \text{ with } |G_\tau|_\infty \leq C(\eta_2, \eta_3)|\nabla\tau|_\infty \,, \text{and} \\
\tau(U - W) &= (\mathbf{I} + H_\tau)(U - W) \,, \text{ with } |H_\tau|_\infty \leq C(\eta_2, \eta_3)|\nabla\tau|_\infty \,.
\end{aligned}$$

It follows that, up to second order $o(|\nabla\tau|_\infty{}^2)$ terms,

$$\begin{aligned}
\tau(\Delta) - \Delta &= \tau(\bar{\mathcal{A}})^{-1}(\tau(U) - \tau(W)) - \bar{\mathcal{A}}^{-1}(U - W) \\
&= \left(\bar{\mathcal{A}}[\mathbf{1} + G_\tau]\right)^{-1}[(\mathbf{I} + H_\tau)(U - W)] - \bar{\mathcal{A}}^{-1}(U - W) \\
&\simeq \bar{\mathcal{A}}^{-1}H_\tau(U - W) + G_\tau\Delta \,.
\end{aligned} \tag{22}$$

By writing $\bar{\mathcal{A}}^{-1}H_\tau = \widetilde{H_\tau}\bar{\mathcal{A}}^{-1}$, and since $\bar{\mathcal{A}}$ is diagonal, we verify that

$$(\widetilde{H_\tau})_{i,j} = (H_\tau)_{i,j}\frac{\mathcal{A}_{i,i}}{\mathcal{A}_{j,j}} \,, \text{with}$$

$\frac{\mathcal{A}_{i,i}}{\mathcal{A}_{j,j}} \leq \eta_1$, and hence that

$$\bar{\mathcal{A}}^{-1}H_\tau(U - W) = \widetilde{H_\tau}\Delta \,, \text{ with } |\widetilde{H_\tau}|_\infty \leq C(\eta_1, \eta_2, \eta_3)|\nabla\tau|_\infty \,. \tag{23}$$

We conclude by combining (22) and (23) into

$$\begin{aligned}
\|(\Delta - \tau(\Delta))x\| &= \|(G_\tau + \widetilde{H_\tau})\Delta x\| \\
&\leq C'(\eta_1, \eta_2, \eta_3)|\nabla\tau|_\infty\|\Delta x\| \,,
\end{aligned}$$

which proves (19) □

C.3 Proof of part (c)

This result is a consequence of the consistency of the cotangent Laplacian to the Laplace-Beltrami operator on S [9]:

Theorem C.3 ([9], Thm 3.4) *Let $\mathcal{M}$ be a compact polyhedral surface which is a normal graph over a smooth surface S with distortion tensor $\mathcal{T}$, and let $\bar{\mathcal{T}} = (\det \mathcal{T})^{1/2}\mathcal{T}^{-1}$. If the normal field uniform distance $d(\mathcal{T}, \mathbf{1}) = \|\bar{\mathcal{T}} - \mathbf{1}\|_\infty$ satisfies $d(\mathcal{T}, \mathbf{1}) \leq \epsilon$, then*

$$\|\Delta_{\mathcal{M}} - \Delta_S\| \leq \epsilon \,. \tag{24}$$

If $\Delta_{\mathcal{M}}$ converges uniformly to Δ_S, in particular we verify that

$$\|x\|_{\mathcal{H}(\mathcal{M})} \to \|x\|_{\mathcal{H}(S)} \,.$$

Thus, given two meshes $\mathcal{M}$, $\mathcal{M}'$ approximating a smooth surface S in terms of uniform normal distance, and the corresponding irregular sampling x and x' of an underlying function $\bar{x} : S \to \mathbb{R}$, we have

$$\|\rho(Ax + B\Delta_{\mathcal{M}}x) - \rho(Ax' + B\Delta_{\mathcal{M}'}x')\| \leq \|A\|\|x - x'\| + \|B\|\|\Delta_{\mathcal{M}}x - \Delta_{\mathcal{M}'}x'\| \,. \tag{25}$$

Since $\mathcal{M}$ and $\mathcal{M}'$ both converge uniformly normally to S and $\bar{x}$ is Lipschitz on S, it results that

$$\|x - \bar{x}\| \leq L\epsilon \,, \text{ and } \|x' - \bar{x}\| \leq L\epsilon \,,$$

thus $\|x - x'\| \leq 2L\epsilon$. Also, thanks to the uniform normal convergence, we also have convergence in the Sobolev sense:

$$\|x - \bar{x}\|_{\mathcal{H}} \lesssim \epsilon \,, \; \|x' - \bar{x}\|_{\mathcal{H}} \lesssim \epsilon \,,$$

which implies in particular that

$$\|x - x'\|_{\mathcal{H}} \lesssim \epsilon \,. \tag{26}$$

From (25) and (26) it follows that

$$\begin{aligned} \|\rho(Ax + B\Delta_{\mathcal{M}}x) - \rho(Ax' + B\Delta_{\mathcal{M}'}x')\| &\leq 2\|A\|L\epsilon + \\ &\quad + \|B\|\|\Delta_{\mathcal{M}}x - \Delta_S\bar{x} + \Delta_S\bar{x} - \Delta_{\mathcal{M}'}x'\| \\ &\leq 2\epsilon\left(\|A\|L + \|B\|\right) \,. \end{aligned} \tag{27}$$

By applying again Lemma C.1 to $\tilde{x} = \rho(Ax + B\Delta_{\mathcal{M}}x)$, $\tilde{x}' = \rho(Ax' + B\Delta_{\mathcal{M}'}x')$, we have

$$\|\tilde{x} - \tilde{x}'\|_{\mathcal{H}} \leq C\|\tilde{x} - \tilde{x}'\|^{\frac{\beta_1 - 1}{\beta_1 - 1/2}} \lesssim \epsilon^{\frac{\beta_1 - 1}{\beta_1 - 1/2}} \,.$$

We conclude by retracing the same argument as before, reapplying Lemma C.1 at each layer to obtain

$$\|\Phi_{\mathcal{M}}(x) - \Phi_{\mathcal{M}'}(x')\| \leq C\epsilon^{\prod_{r=1}^{R} \frac{\beta_r - 1}{\beta_r - 1/2}} \,. \;\square \,.$$

D Proof of Corollary 4.3

We verify that

$$\begin{aligned}\|\rho(B\Delta x) - \rho(B\tau(\Delta)\tau(x))\| &\leq \|B\|\|\Delta x - \tau(\Delta)\tau(x)\| \\ &\leq \|B\|\|\Delta(x-\tau(x)) + (\Delta - \tau(\Delta))(\tau(x))\| \\ &\leq \|B\|(\|\Delta(x-\tau(x))\| + \|(\Delta - \tau(\Delta))(\tau(x))\| \,.\end{aligned}$$

The second term is $o(|\nabla\tau|_\infty)$ from Lemma C.2. The first term is

$$\|x - \tau(x)\|_{\mathcal{H}} \leq \|\Delta(\mathbf{I} - \tau)\|\|x\| \leq \|\nabla^2\tau\|\|x\| \,,$$

where $\|\nabla^2\tau\|$ is the uniform Hessian norm of τ. The result follows from applying the cascading argument from last section. □

E Preliminary Study: Metric Learning for Dense Correspondence

As an interesting extension, we apply the architecture we built in Experiments 6.2 directly to a dense shape correspondence problem.

Similarly as the graph correspondence model from [8], we consider a Siamese Surface Network, consisting of two identical models with the same architecture and sharing parameters. For a pair of input surfaces $\mathcal{M}_1, \mathcal{M}_2$ of N_1, N_2 points respectively, the network produces embeddings $E_1 \in \mathbb{R}^{N_1 \times d}$ and $E_2 \in \mathbb{R}^{N_2 \times d}$. These embeddings define a trainable similarity between points given by

$$s_{i,j} = \frac{e^{\langle E_{1,i}, E_{2,j} \rangle}}{\sum_{j'} e^{\langle E_{1,i}, E_{2,j'} \rangle}}, \tag{28}$$

which can be trained by minimizing the cross-entropy relative to ground truth pairs. A diagram of the architecture is provided in Figure 2.

In general, dense shape correspondence is a task that requires a blend of intrinsic and extrinsic information, motivating the use of data-driven models that can obtain such tradeoffs automatically. Following the setup in Experiment 6.2, we use models with 15 ResNet-v2 blocks with 128 output features each, and alternate Laplace and Dirac based models with Average Pooling blocks to cover a larger context: The input to our network consists of vertex positions only.

We tested our architecture on a reconstructed (i.e. changing the mesh connectivity) version of the real scan of FAUST dataset[1]. The FAUST dataset contains 100 real scans and their corresponding ground truth registrations. The ground truth is based on a deformable template mesh with the same ordering and connectivity, which is fitted to the scans. In order to eliminate the bias of using the same template connectivity, as well as the need of a single connected component, the scans are reconstructed again with [5]. To foster replicability, we release the processed dataset in the additional material. In our experiment, we use 80 models for training and 20 models for testing.

Since the ground truth correspondence is implied only through the common template mesh, we compute the correspondence between our meshes with a nearest neighbor search between the point cloud and the reconstructed mesh. Consequently, due to the drastic change in vertex replacement after the remeshing, only 60-70 percent of labeled matches are used. Although making it more challenging, we believe this setup is close to a real case scenario, where acquisition noise and occlusions are unavoidable.

Our preliminary results are reported in Figure 3. For simplicity, we generate predicted correspondences by simply taking the mode of the softmax distribution for each reference node i: $\hat{j}(i) = \arg\max_j s_{i,j}$, thus avoiding a refinement step that is standard in other shape correspondence pipelines. The MLP model uses no context whatsoever and provides a baseline that captures the prior information from input coordinates alone. Using contextual information (even extrinsically as in point-cloud model) brings significative improvments, but these results may be substantially improved by encoding further prior knowledge. An example of the current failure of our model is depitcted in Figure 5, illustrating that our current architecture does not have sufficiently large spatial context to disambiguate between locally similar (but globally inconsistent) parts.

We postulate that the FAUST dataset [1] is not an ideal fit for our contribution for two reasons: (1) it is small (100 models), and (2) it contains only near-isometric deformations, which do not require the generality offered by our network. As demonstrated in [7], the correspondence performances can be dramatically improved by constructing basis that are invariant to the deformations. We look forward to the emergence of new geometric datasets, and we are currently developing a capture setup that will allow us to acquire a more challenging dataset for this task.

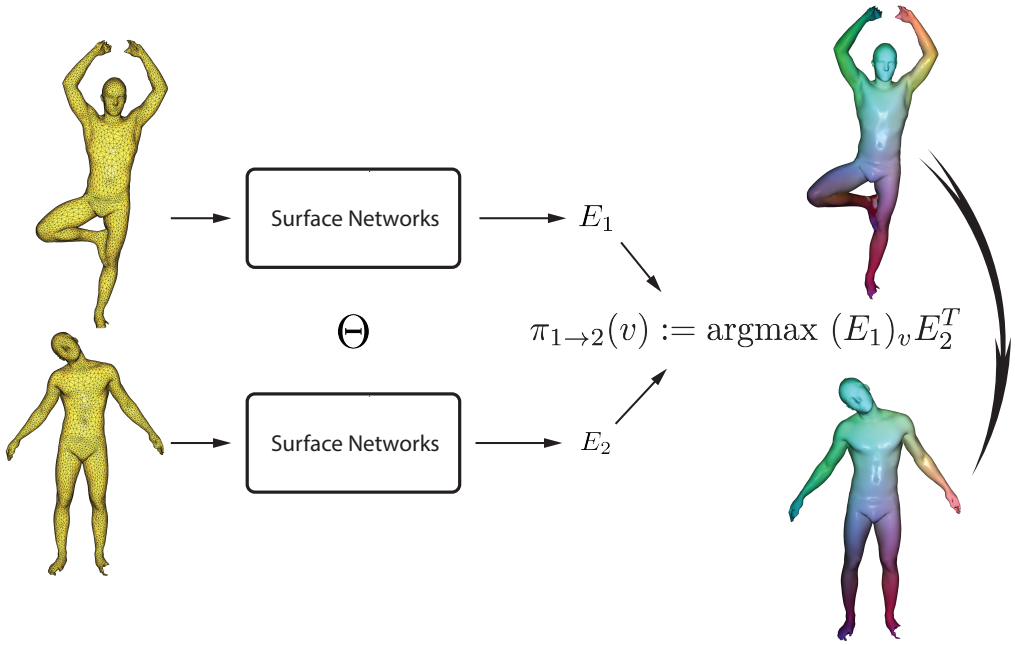

Figure 2: Siamese network pipeline: the two networks take vertex coordinates of the input models and generate a high dimensional feature vector, which are then used to define a map from $\mathcal{M}_1$ to $\mathcal{M}_2$. Here, the map is visualized by taking a color map on $\mathcal{M}_2$, and transferring it on $\mathcal{M}_1$

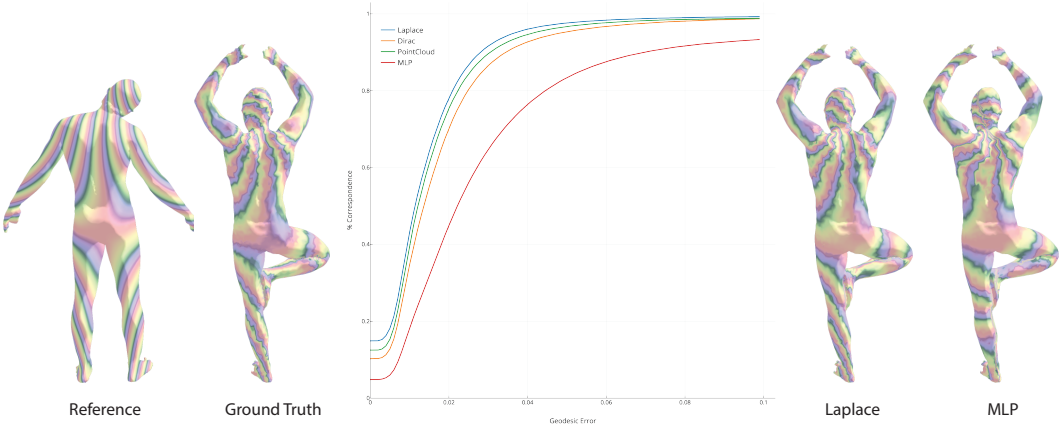

Figure 3: Additional results from our setup. Plot in the middle shows rate of correct correspondence with respect to geodesic error [6]. We observe that Laplace is performing similarly to Dirac in this scenario. We believe that the reason is that the FAUST dataset contains only isometric deformations, and thus the two operators have access to the same information. We also provide visual comparison, with the transfer of a higher frequency colormap from the reference shape to another pose.

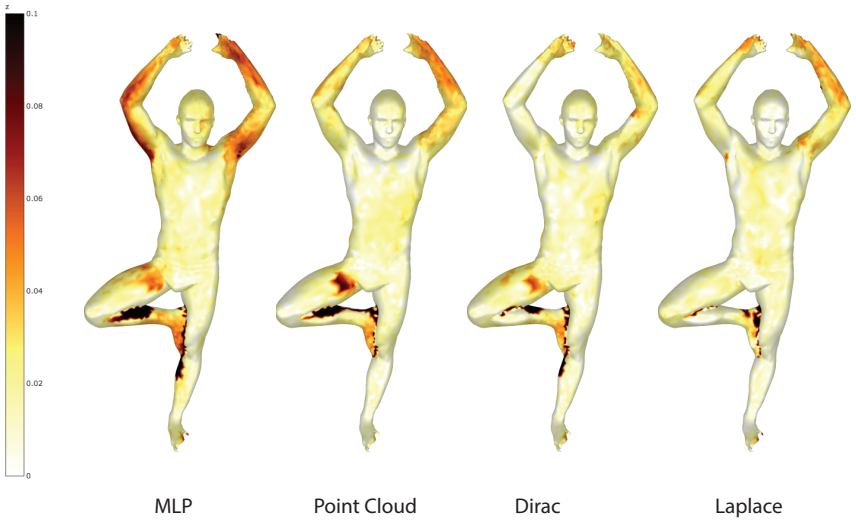

Figure 4: Heat map illustrating the point-wise geodesic difference between predicted correspondence point and the ground truth. The unit is proportional to the geodesic diameter, and saturated at 10%.

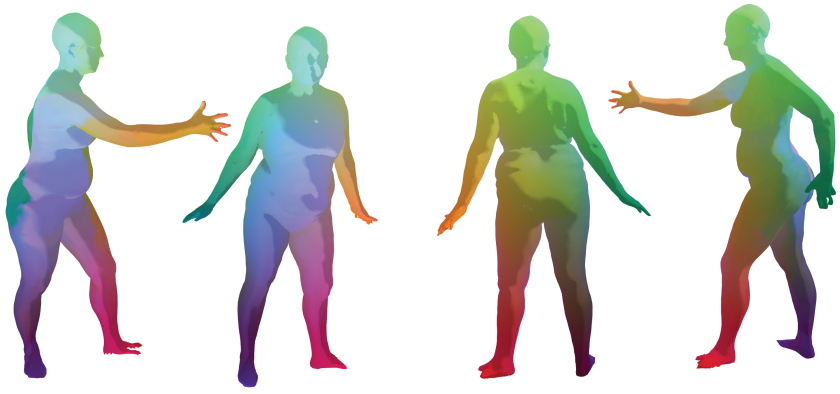

Figure 5: A failure case of applying the Laplace network to a new pose in the FAUST benchmark dataset. The network confuses between left and right arms. We show the correspondence visualization for front and back of this pair.

F Further Numerical Experiments

Figure 6: Qualitative comparison of different models. We plot 1th, 10th, 20th, 30th and 40th predicted frame correspondingly.

Figure 7: Qualitative comparison of different models. We plot 1th, 10th, 20th, 30th and 40th predicted frame correspondingly.

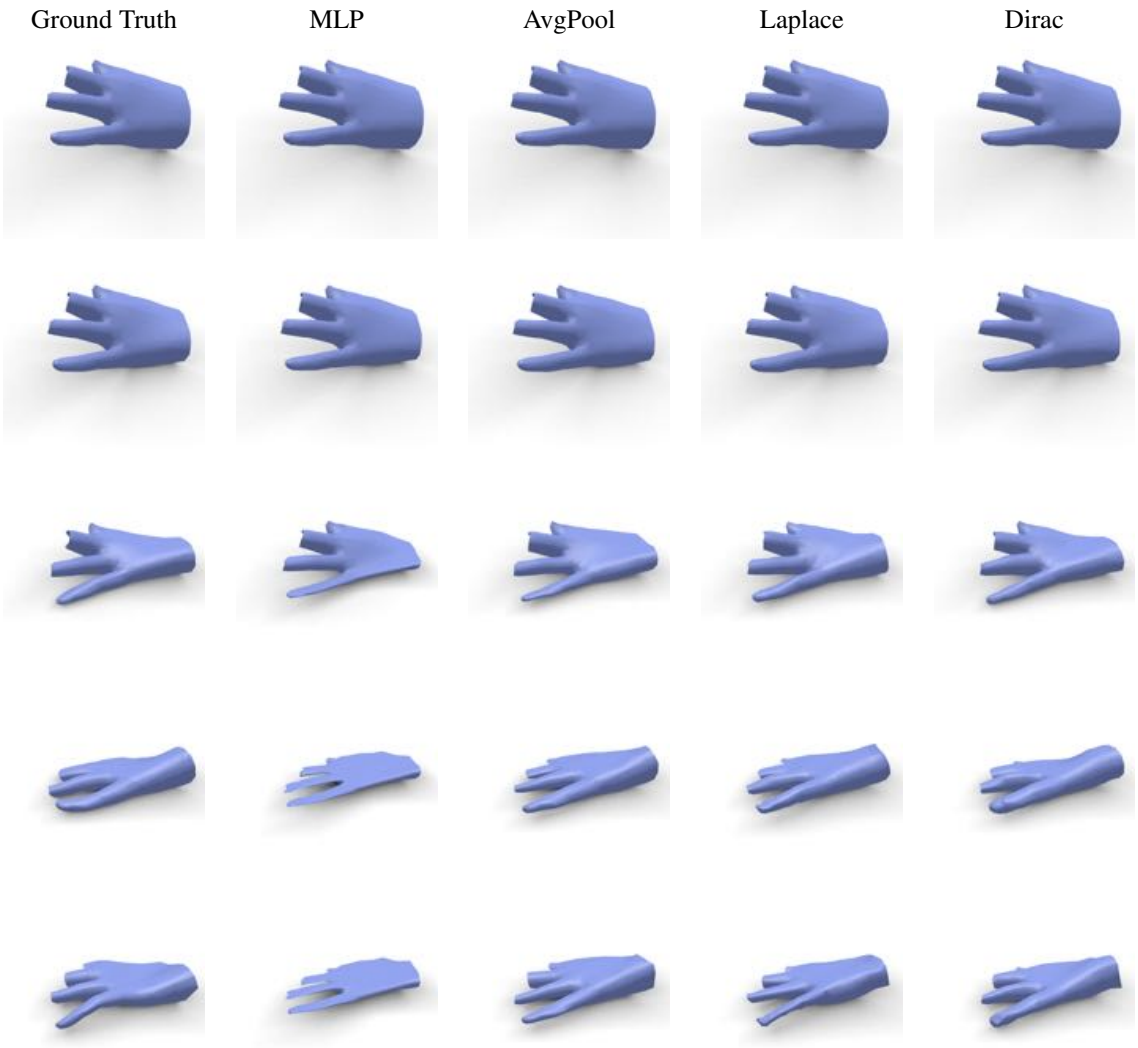

Figure 8: Qualitative comparison of different models. We plot 1th, 10th, 20th, 30th and 40th predicted frame correspondingly.

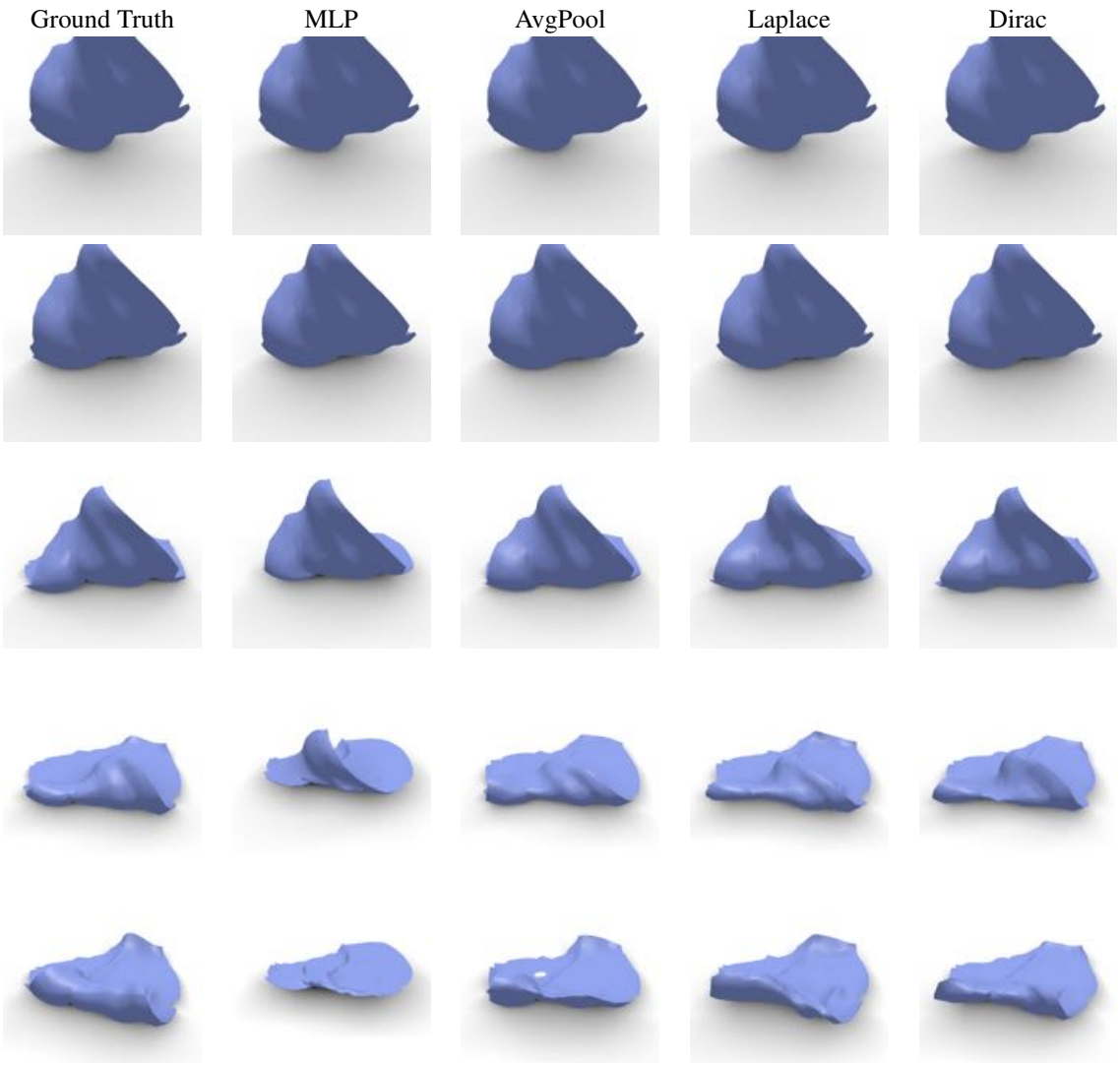

Figure 9: Qualitative comparison of different models. We plot 1th, 10th, 20th, 30th and 40th predicted frame correspondingly.

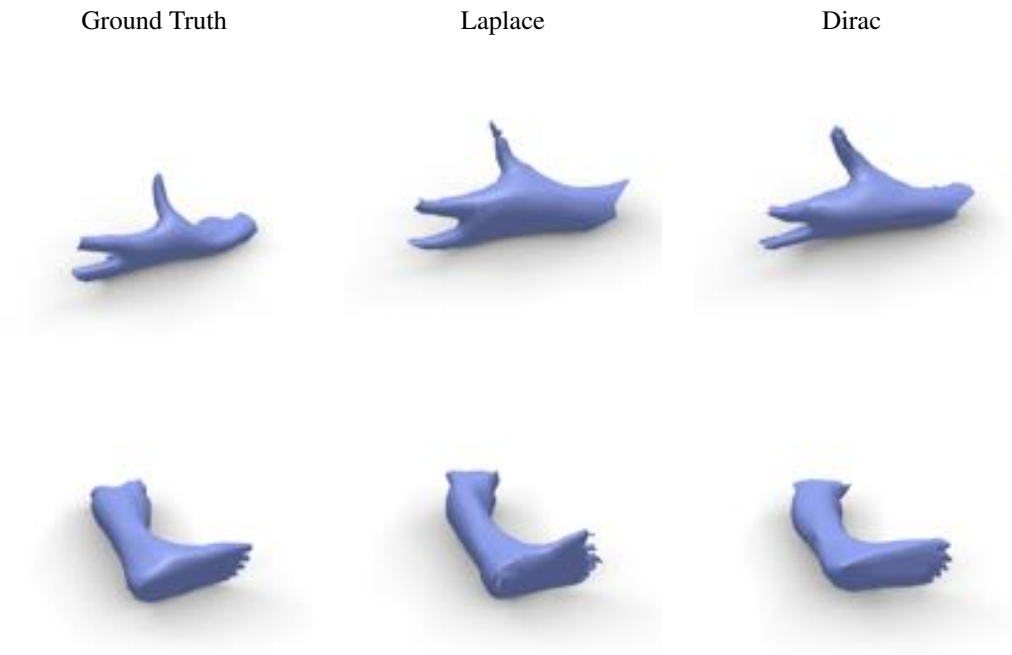

Figure 10: Dirac-based model visually outperforms Laplace-based models in the regions of high mean curvature.

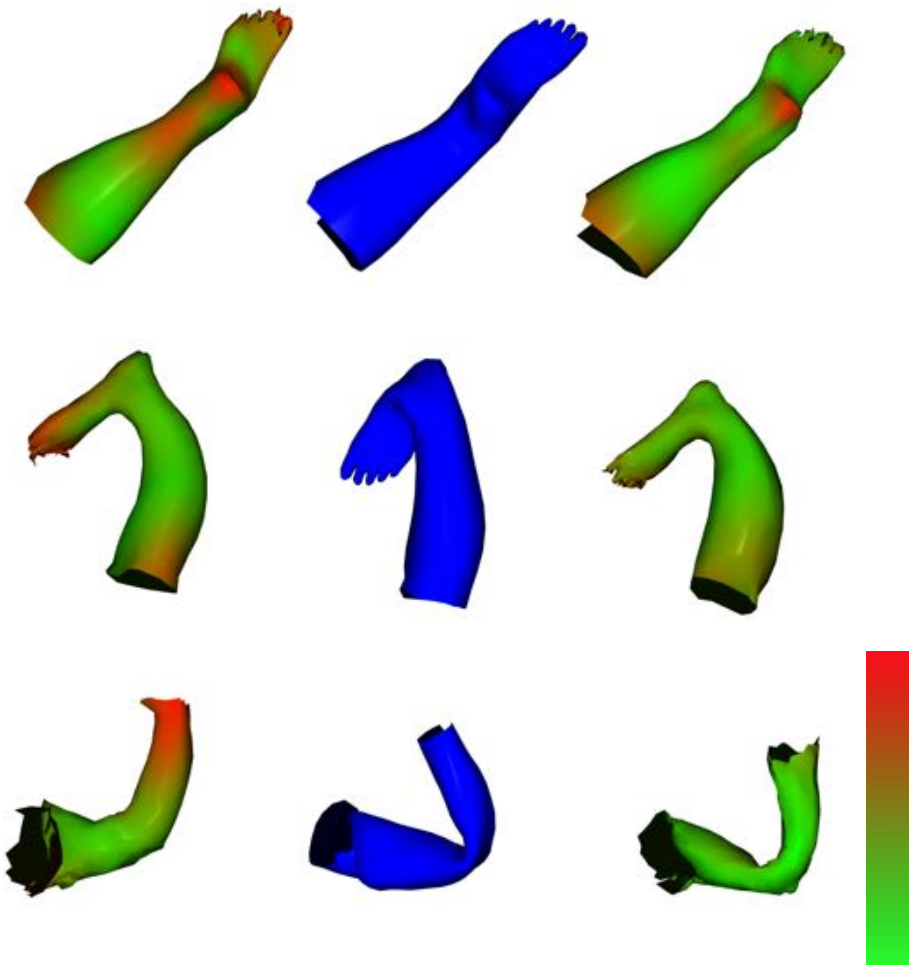

Figure 11: From left to right: Laplace, ground truth and Dirac based model. Color corresponds to mean squared error between ground truth and prediction: green - smaller error, red - larger error.

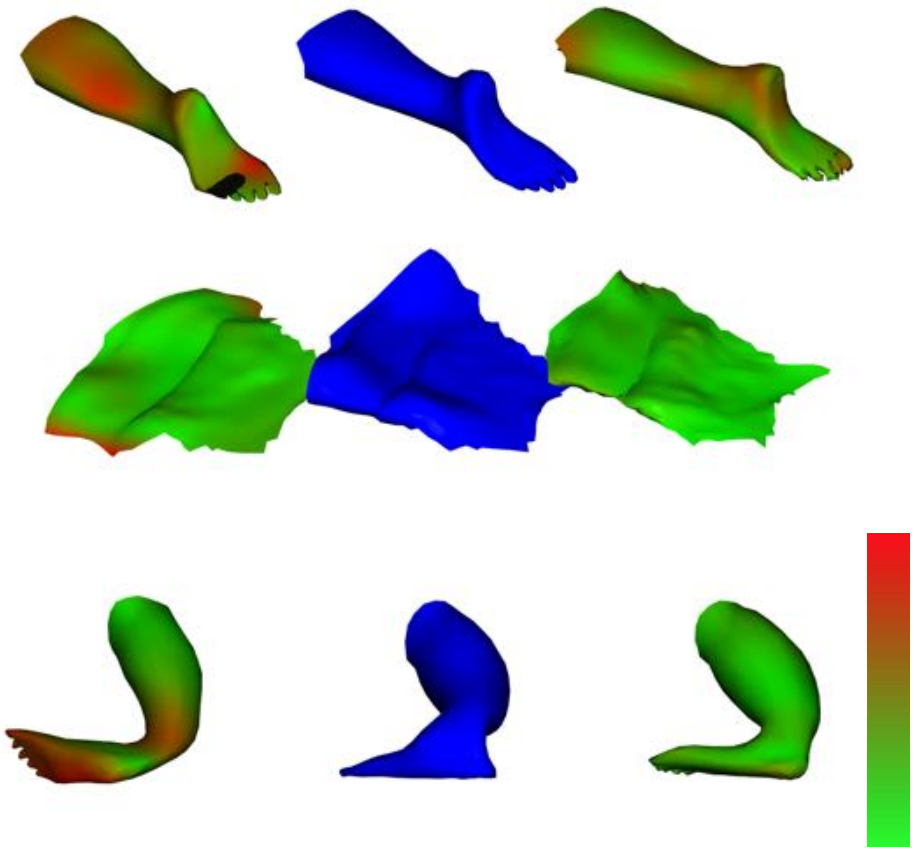

Figure 12: From left to right: set-to-set, ground truth and Dirac based model. Color corresponds to mean squared error between ground truth and prediction: green - smaller error, red - larger error.

References

[1] F. Bogo, J. Romero, M. Loper, and M. J. Black. Faust: Dataset and evaluation for 3d mesh registration. In *Proceedings of the IEEE Conference on Computer Vision and Pattern Recognition*, pages 3794–3801, 2014. 10

[2] M. M. Bronstein, J. Bruna, Y. LeCun, A. Szlam, and P. Vandergheynst. Geometric deep learning: going beyond euclidean data. *arXiv preprint arXiv:1611.08097*, 2016. 3

[3] D. Chen and J. R. Gilbert. Obtaining bounds on the two norm of a matrix from the splitting lemma. *Electronic Transactions on Numerical Analysis*, 21:28–46, 2005. 4

[4] K. C. Das. Extremal graph characterization from the upper bound of the laplacian spectral radius of weighted graphs. *Linear Algebra and Its Applications*, 427(1):55–69, 2007. 2

[5] Y. Hu, Q. Zhou, X. Gao, A. Jacobson, D. Zorin, and D. Panozzo. Tetrahedral meshing in the wild. *Submitted to ACM Transaction on Graphics*, 2018. 10

[6] V. G. Kim, Y. Lipman, and T. Funkhouser. Blended intrinsic maps. In *ACM Transactions on Graphics (TOG)*, volume 30, page 79. ACM, 2011. 11

[7] O. Litany, T. Remez, E. Rodolà, A. M. Bronstein, and M. M. Bronstein. Deep functional maps: Structured prediction for dense shape correspondence. *2017 IEEE International Conference on Computer Vision (ICCV)*, pages 5660–5668, 2017. 10

[8] A. Nowak, S. Villar, A. S. Bandeira, and J. Bruna. A note on learning algorithms for quadratic assignment with graph neural networks. *arXiv preprint arXiv:1706.07450*, 2017. 10

[9] M. Wardetzky. Convergence of the cotangent formula: An overview. In *Discrete Differential Geometry*, pages 275–286. 2008. 2, 8